Motion Planning and Feedback Control for Bipedal Robots Riding a Snakeboard

Jonathan Anglingdarma, Ayush Agrawal, Joshua Morey and Koushil Sreenath

***Abstract*— This paper formulates a methodology to plan and control flat-terrain motions of an underactuated bipedal robot riding a snakeboard, which is a steerable variant of the skateboard. We use tools from non-holonomic motion planning to study snakeboard gaits and develop feedback control strategies that enable bipedal robots to produce the desired gaits while maintaining balance, regulating the magnitude and direction of the velocity of the snakeboard, achieving sharp turns, and avoiding obstacles.**

I. Introduction

Legged robots are highly versatile machines that exhibit a wide variety of locomotion modes like walking, running and jumping which enable them to traverse over extremely rough terrain unlike wheeled robots. On flat terrain however, wheeled robots outperform their legged counterparts in both, speed and energy efficiency. This paper attempts to bridge this performance gap by introducing a faster and efficient alternative to legged locomotion on flat terrain - *riding a passive wheeled platform*. With this research, we hope to optimize the ability of legged robots by offering them a medium where they could use a wheeled platform to travel faster on smooth terrains while also having the option to walk or run in more challenging terrain. In particular, we develop control strategies for a high degree-of-freedom and underactuated bipedal robot, Cassie[1] to autonomously ride an *unpowered* wheeled platform known as the snakeboard as illustrated in Fig. 1.

The snakeboard is composed of a central bar that connects two rotating pads where the rider places their feet. These rotating foot-pads are connected to the axles of the wheels and allow the rider to independently steer the wheels. Unlike a skateboard, the snakeboard allows the users to propel themselves by rotating their body and the foot-pads, without the need for placing their feet on the ground. By interacting with the snakeboard pads through different gait patterns, the rider can achieve various motions in the inertial frame.

A. Challenges

Enabling a bipedal robot to safely ride a snakeboard involves many challenges. First, snakeboards are highly dynamic platforms that are sensitive to the input forces and thus, being able to balance on them is challenging. Second, Cassie can only control the snakeboard motion when the contact between its feet and the board is sustained and no slip occurs. Therefore motion plans and control design should provide these additional guarantees. Third, rapid modulation of torso yaw momentum is a critical component in snakeboard propulsion. Since Cassie is arm-less, this ability is severely constrained. These limitations restrict the range of feasible gaits for riding the snakeboard. Cassie is also a high degree-of-freedom, under-actuated robot making the system challenging to control. In addition, riding a snakeboard also requires achieving multiple tasks such as oscillating the hip joints, leaning the body forwards or sideways, and maintaining stable balance. In order to address these challenges and successfully execute dynamic flat-terrain motion plans, we propose an operational space controller that allows Cassie to achieve multiple tasks, while also maintaining friction constraints between the foot and the snakeboard pads.

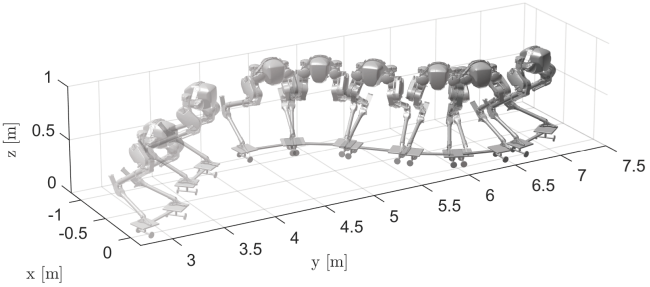

Fig. 1: Cassie Riding a snakeboard along a sinusoidal path. A video of the simulation results can be found here: `https://youtu.be/fapcnAvYbko`

B. Related works

Multi-modal locomotion, and in particular, combining wheeled and legged locomotion is an active area of research. There is a great variety in the types of systems that are paired, the control methodologies used, and how contact between legs and wheels is enforced. For instance, the authors in [1] integrated and successfully demonstrated wheeled locomotion of Cassie with hovershoes and with segways in [2]. The work with ANYmal in [3], is another example of multi-modal locomotion which combines the advantages of both walking and using wheels at its feet. Ascento [4], is also a mobility robot that uses a combination of legs and wheels to maneuver quickly on flat terrain while also being able

This work is supported in part by National Science Foundation Grant CMMI-1944722.

The authors are with Department of Mechanical Engineering, University of California at Berkeley `jonathan_ang@berkeley.edu`, `ayush.agrawal@berkeley.edu`, `joshuamorey@berkeley.edu`, `koushils@berkeley.edu`

[1]Cassie is a bipedal robotic platform developed by Agility Robotics `https://www.agilityrobotics.com/robots#cassie`.

to jump and avoid obstacles. Quattroped [5] is a quadruped robot that can transform its legs to wheels which can be utilized for better performance and efficiency for different ground locomotion platforms.

With regards to combining legged locomotion with passive wheeled devices, [6] considers the problem of stabilizing a planar bipedal robot on a ball. In [7], the authors present an MPC framework to manipulate a ball using a quadruped robot to follow desired trajectories. The work in [8] develops a framework for a 3D humanoid robot to ride a passive skateboard.

The snakeboard considered in this paper is a dynamical system with non-holonomic constraints and motion planning for such systems has been extensively studied in prior work, beginning with [9] that considered various sinusoidal gaits for the snakeboard joints which was later extended to an optimal control framework in [10]. The work in [11], [12] formulated the motion planning problem of steering the snakeboard to a desired goal location by considering various kinematic trajectories. In [13], the authors propose a gait generation technique to achieve displacement along a given direction and present an analytical framework in [14] for the joint configurations to follow desired trajectories in the task space. In [15], the authors consider the problem of trajectory planning by considering only the local curvature of the desired path and in [16] analyze the snakeboard with viscous friction. In [17], the authors analyze human riders on a waveboard, which is another form of a system with non-holonomic constraints.

C. Primary Contributions

Our work draws motivation primarily from the studies made in the non-holonomic motion planning for snakeboards [9] and a force balance control strategy for bipedal robots [18]. In this paper, we modify gaits so that Cassie could achieve some desired features for trajectory planning and compute the desired center-of-mass for Cassie to still be able to maintain its balance while riding on the snakeboard.

Distinct from prior work in [3], [4], [5] which consider the wheels to be fixed to the legs or [1], [2] which consider combining powered wheeled devices with legged robots, we present a trajectory planning and optimization-based feedback controller for a bipedal robot, Cassie to ride a passive wheeled platform, the *snakeboard*. Through our proposed framework, the combined Cassie-snakeboard system is able to follow desired trajectories in the task-space, achieve sharp turns and avoid obstacles, while maintaining balance and friction constraints.

D. Organization

The rest of the paper is organized as follows. Section II describes the dynamical model of Cassie integrated with the snakeboard. Section III discusses different approaches for generating various gaits to propel the snakeboard along different desired trajectories. Section IV presents a balance control strategy for Cassie to be able to achieve the different gaits and regulate the center-of-mass and angular velocities of the snakeboard. Section V presents results from numerical simulations for various scenarios such as obstacle avoidance, achieving sharp turns and tracking desired velocities. Section VII summarizes the work explored in this paper and describes future directions.

TABLE I: Physical parameters of the snakeboard.

Symbol	Description
m_s	mass of the snakeboard
m_r	mass of the rotor
J	inertia of the snakeboard
J_r	inertia of the rotor
J_w	inertia of the wheels
l	length from the snakeboard's center-of-mass to the wheels

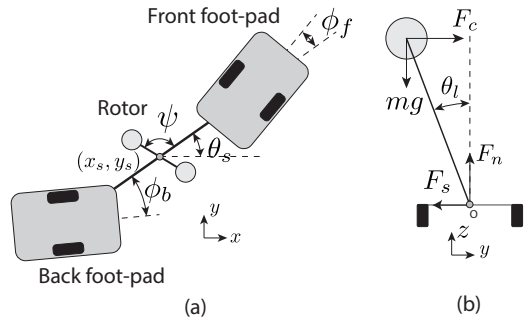

Fig. 2: Simplified model of a snakeboard. (a) Snakeboard as viewed from top. (b) Rotor lean angle in the lateral direction of the snakeboard.

II. Dynamical Model of Cassie on a Snakeboard

With the challenges described above, this section investigates the dynamical model of Cassie, snakeboard and how they interact with one another.

A. Dynamical Model of Cassie

Cassie is a 20-dimensional bipedal robot with 10 degrees of actuation and the dynamics can be expressed as

$$D\ddot{q}_c + C\dot{q}_c + G = B\tau + J_s^T \tau_s + J_c^T f_c, \tag{1}$$

where $q_c \in \mathbb{R}^{20}$ is the configuration of the robot, $D \in \mathbb{R}^{20\times 20}$ is the inertia matrix, $C \in \mathbb{R}^{20\times 20}$ is the Coriolis matrix, $G \in \mathbb{R}^{20}$ is the generalized gravity vector, $B \in \mathbb{R}^{20\times 10}$ is the actuation distribution matrix, $\tau_s \in \mathbb{R}^4$ are the spring torques, J_s is the jacobian of the spring deflections, $\tau \in \mathbb{R}^{10}$ are the input joint torques, $f_c \in \mathbb{R}^{12}$ are the contact forces and $J_c \coloneqq \begin{bmatrix} J_{c,1}^T \cdots J_{c,4}^T \end{bmatrix}^T \in \mathbb{R}^{12\times 20}$ is the jacobian of the contact positions. For later use, we define $\bar{J}_c \coloneqq \begin{bmatrix} J_{c,1}^T B \cdots J_{c,4}^T B \end{bmatrix}^T \in \mathbb{R}^{12\times 10}$. The configuration variables q consist of the position of the robot, the orientation $\varepsilon \coloneqq \begin{bmatrix} \theta_c & \psi_c & \phi_c \end{bmatrix}^T$ of the pelvis represented in Z-Y-X euler angles and the joint angles. These are detailed in [19]. In later sections, we will particularly use the yaw of the pelvis θ_c and the *hip yaw* angles denoted by $q_{hip} \coloneqq \begin{bmatrix} q_{hip,b} & q_{hip,f} \end{bmatrix}^T$ corresponding to the legs on the back and front foot-pads of the snakeboard.

B. Simplified Dynamical Model of Snakeboard

For the purpose of path planning, we derive a simplified dynamical model of the snakeboard from [9]. Figure 2 depicts this model which consists of a rotor at the center of the snakeboard to model a rider rotating their body. The configuration variables of the snakeboard q_s include the inertial position x_s, y_s, orientation θ_s, the angles of the front and back foot-pads ϕ_f and ϕ_b, and the relative angle of the rotor with the snakeboard ψ. The various physical parameters of the snakeboard are mentioned in Table I. Assuming wheels do not slip sideways, non-holonomic constraints (2), (3) are imposed on the snakeboard,

$$-\sin(\phi_b+\theta_s)\dot{x}_s+\cos(\phi_b+\theta_s)\dot{y}_s-l\dot{\theta}_s\cos\phi_b=0, \quad (2)$$

$$-\sin(\phi_f+\theta_s)\dot{x}_s+\cos(\phi_f+\theta_s)\dot{y}_s-l\dot{\theta}_s\cos\phi_f=0. \quad (3)$$

With the motion of the snakeboard restricted to level ground, the potential energy of the snakeboard remains constant and the Lagrangian dynamics for the snakeboard are based solely on the kinetic energy. The equations of motion of the snakeboard [9] are then obtained as

$$\ddot{x}_s=\frac{1}{m_s+m_r}\left(\lambda_1\sin(\phi_b+\theta_s)+\lambda_2\sin(\phi_f+\theta_s)\right), \quad (4)$$

$$\ddot{y}_s=-\frac{1}{m_s+m_r}\left(\lambda_1\cos(\phi_b+\theta_s)+\lambda_2\cos(\phi_f+\theta_s)\right), \quad (5)$$

$$\ddot{\theta}_s=\frac{1}{J}\left(-u_1-u_2-u_3+\lambda_1 l\cos\phi_b-\lambda_2 l\cos\phi_f\right), \quad (6)$$

$$\ddot{\psi}=\frac{1}{J_r}\left(u_1-J_r\ddot{\theta}_s\right), \quad (7)$$

$$\ddot{\phi}_b=\frac{1}{J_w}\left(u_2-J_w\ddot{\theta}_s\right), \quad (8)$$

$$\ddot{\phi}_f=\frac{1}{J_w}\left(u_3-J_w\ddot{\theta}_s\right), \quad (9)$$

where u_1, u_2 and u_3 are the input torques at the joints corresponding to the configuration variables ψ, ϕ_b and ϕ_f respectively, and λ_1 and λ_2 are Lagrange multipliers that arise due to the non-holonomic constraints in (2) and (3). The particular solution for λ_1 and λ_2 can be found in [9].

Remark 1. *The variables ψ, ϕ_b and ϕ_f correspond to the local configuration of the snakeboard that the rider has control over. The variables x_s, y_s and θ_s correspond to the configuration of the snakeboard in the inertial frame. Due to the non-holonomic constraints in* (2) *and* (3)*, by modulating the local configuration variables, the rider can cause a desired net change in the inertial frame.*

C. Contact Model between Cassie and the Snakeboard

In Section II, we used a model of the snakeboard where the rotor was used as a simplification of the dynamics of the rider [9]. While this simplified model is useful for path planning of the snakeboard, it does not capture the true dynamics of the rider. In particular, the dynamics of the rider (here, Cassie) are given by the robot dynamics in Section II-A and the inputs to the snakeboard u_j, $j\in\{1,2,3\}$ are determined by

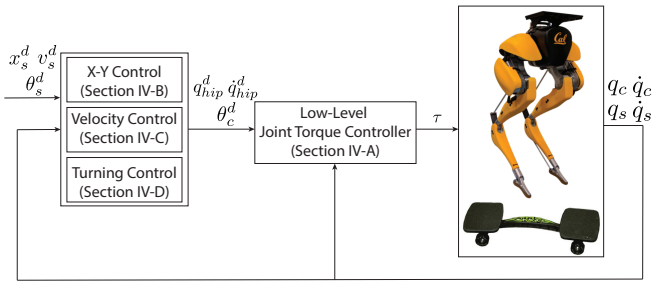

Fig. 3: Feedback control diagram. Here q_c represents Cassie's states and q_s represents the snakeboard's states

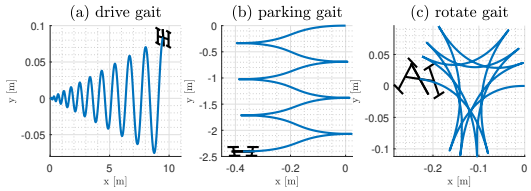

Fig. 4: Trajectory of the center-of-mass of the simplified snakeboard model for various gaits, all with 0 initial velocity.

the contact forces between the foot and the snakeboard pads as

$$u_1=\begin{bmatrix}0 & 0 & 1\end{bmatrix}\Sigma_{i=1}^{4} r_i^c\times -f_c^i, \quad (10)$$

$$u_2=\begin{bmatrix}0 & 0 & 1\end{bmatrix}\Sigma_{i=1}^{2} r_i^{fp}\times -f_c^i, \quad (11)$$

$$u_3=\begin{bmatrix}0 & 0 & 1\end{bmatrix}\Sigma_{i=3}^{4} r_i^{fp}\times -f_c^i, \quad (12)$$

where r_i^{fp} represents the i^{th} location of the contact point with respect to the foot-pads, r_i^c denotes the i^{th} location of the contact point with respect to center-of-mass of the snakeboard, f_c^i denotes the contact forces at the i^{th} contact point, with $i=1,2$ representing the back foot-pads and $i=3,4$ representing the front foot-pads of the snakeboard.

III. Path Planing and Gait Generation

As mentioned in Remark 1, a desired net change in the global position and orientation of the snakeboard can be achieved by regulating the local coordinates of the snakeboard and the problem of trajectory planning of the snakeboard turns into a problem of gait generation of the shape variables. We define a *trajectory* of the snakeboard in the global frame as the tuple $(x_s(t),y_s(t),\theta_s(t))$ denoting the global positions and orientation of the snakeboard, and a *gait* as the tuple $(\psi(t),\phi_b(t),\phi_f(t))$ denoting the shape variables at time $t\in[0,T]$ for $T>0$.

For the sake of completeness, we present below the results in [9] and illustrate the effects of different gaits on the trajectories in the global frame. Consider the following time-varying sinusoidal inputs for the simplified model snakeboard in (7), (8), (9)

$$u_i=a_i\sin(w_i t),\ i\in\{1,2,3\}, \quad (13)$$

where the parameters of the sinusoids for various trajectories are presented in Table II. The drive gait (Fig. 4a) propels the snakeboard forward or backward depending on the phase

TABLE II: Gait parameters for different gaits from [9].

Parameter	Drive Gait	Parking Gait	Rotate Gait
a_1	0.3 rad	1 rad	1 rad
w_1	1 rad/s	3 rad/s	2 rad/s
a_2,$-a_3$	0.3 rad	1 rad	1 rad
w_2,w_3	1 rad/s	2 rad/s	1 rad/s

difference between the foot-pads and the rotor. The parking gait (Fig. 4b) results in a net displacement along the lateral direction. The rotate gait (Fig. 4c) results in a net change in orientation of the snakeboard with very small displacement in both, x and y directions.

Remark 2. *The distinguishing factor of the drive gait from other gaits is the equal frequencies for both, the foot-pads and the rotor. In the following sections, we will particularly make use of the drive gait presented here on the simplified snakeboard model to formulate a gait planner for Cassie to follow various trajectories.*

IV. Control Design

Having presented the gait generation technique for the snakeboard using the simplified model, in this section, we discuss the low-level control strategy implemented on Cassie in order to achieve the desired trajectory while still being able to balance on the snakeboard.

A. Low-Level Joint Controller

Our low-level feedback controller is derived from [18] which presents an optimization-based framework to obtain desired forces $f_c^d = \begin{bmatrix} f_{c,1}^{d\,T} & \cdots & f_{c,4}^{d\,T} \end{bmatrix}^T \in \mathbb{R}^{12}$ at the four contact points that stabilizes the center-of-mass position $r_c \in \mathbb{R}^3$ and velocity $\dot{r}_c$ of the robot as well as the orientation ε and rotational velocity $\dot{\varepsilon}$ of the pelvis to desired values r_c^d, $\dot{r}_c^d$, ε^d and $\dot{\varepsilon}^d$. This is achieved by considering a fictitious wrench $F_{com} \in \mathbb{R}^6$ at a frame coincident with the center-of-mass of the robot and parallel to the orientation of the pelvis,

$$F_{com} = \begin{bmatrix} m_c g \mathbf{e}_3 - K_p(r_c - r_c^d) - D_p(\dot{r}_c - \dot{r}_c^d) \\ R\left(-2\left(\delta \mathbb{I} + \hat{\xi}\right) K_r \xi - D_r\left(\omega - \omega^d\right)\right) \end{bmatrix}, \qquad (14)$$

where $\mathbf{e}_3 = \begin{bmatrix} 0 & 0 & 1 \end{bmatrix}^T$, R is the equivalent rotation matrix representation of the orientation of the pelvis given by $R = R_z(\theta_c)R_y(\gamma_c)R_x(\phi_c)$, with R_z, R_y and R_x denoting the rotations about the Z, Y and X axes respectively. The rotation matrix R^d corresponding to the desired orientation can be similarly obtained. The terms ξ and δ denote the vector and scalar part of the quaternion corresponding to the orientation error $R^{dT}R$. Additionally, ω and ω^d denote the actual and desired body angular velocities of the pelvis respectively, which can be obtained from the euler angles and their velocities. The desired height r_c^d with respect to the snakeboard is kept at a constant value and the desired yaw of the robot's pelvis with respect to the snakeboard is a sinusoidal function as in (13).

The center-of-mass wrench F_{com} can be transformed to equivalent contact forces f_c^d through the *grasp map* G_c and wrench basis W as, $F_{com} = G_c W f_c^d$, where the *wrench basis* W is required to transform a force $f_{c,i}^d$ at a contact point to an equivalent wrench $F_c^i = \begin{bmatrix} f_{c,i}^{d\,T} & \mathbf{0}_{3\times1}^T \end{bmatrix}^T$. The desired contact forces can then be obtained by finding the minimizer of $\|F_{com} - G_c W f_c^d\|^2$. However, in order to oscillate the foot-pads of the snakeboard as in (13), we require the legs of Cassie to follow a sinusoidal trajectory, in addition to maintaining a desired center-of-mass position and orientation of the pelvis. We also require that the feet do not slip on the foot-pads. We achieve this by formulating the feedback control as the following optimization problem,

$$\begin{aligned} \min_{f_c^d, \tau} \; & \|F_{com} - G_c W f_c^d\|_{W_F}^2 + \|\tau_{hip} - \tau_{hip}^d\|_{W_\tau}^2 + \|\tau + \bar{J}_c^T f_c^d\|_{W_\delta}^2 \\ \text{s.t. } & f_c^d \in \mathscr{K}_{fric}, \\ & -\bar{\tau} \le \tau \le \bar{\tau}, \end{aligned} \qquad (15)$$

where $\tau_{hip} \in \mathbb{R}^2$ are the torques at the hip yaw joints, $\bar{\tau} \in \mathbb{R}^{10}$ denotes the joint torque limits on Cassie, $\mathscr{K}_{fric}$ corresponds to the linearized friction cone constraints [20] and τ_{hip}^d is given by the linear feedback term,

$$\tau_{hip}^d = -K_{hip}(q_{hip} - q_{hip}^d) - D_{hip}(\dot{q}_{hip} - \dot{q}_{hip}^d), \qquad (16)$$

where $q_{hip}^d = \begin{bmatrix} q_{hip,f}^d & q_{hip,b}^d \end{bmatrix}^T \in \mathbb{R}^2$ and $\dot{q}_{hip}^d$ are desired sinusoidal trajectories for the hip joint angles and velocities on the front and the rear foot-pads, K_{hip} and D_{hip} are appropriate feedback gains. The term $\|\tau + \bar{J}_c^T f_c^d\|_{W_\delta}^2$ in the cost function captures the quasi-static relationship $\tau = -\bar{J}_c^T f_c^d$ between the joint torques and the contact forces.

Remark 3. *As mentioned earlier, due to the lack of arms and an upper torso, Cassie has limited control over the yaw momentum which limits the types of trajectories and*

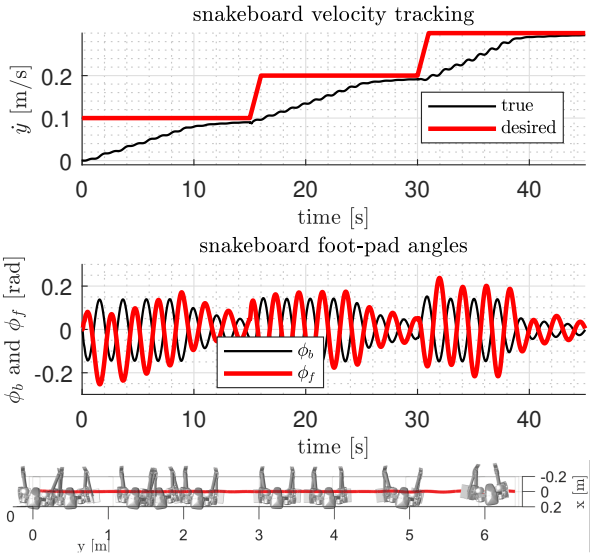

Fig. 5: Results for velocity tracking simulation in Section V-A. Top: Velocity tracking results with the Cassie-snakeboard system initially at rest. Middle: Foot-pad angles of the snakeboard. Bottom: Center-of-mass position of the snakeboard follows a nearly straight line.

behaviors that Cassie can execute with the snakeboard. In the following sections, we will specifically use the ***drive*** *gait presented in Section III. In addition, while* (13) *considers sinusoids for the input torques u_i of the simplified snakeboard dynamics, in the next sections, we will instead consider sinusoidal trajectories for the desired hip angles $q^d_{hip}(t)$ and desired pelvis yaw $\theta^d_c(t)$. We also make an assumption that the feet do not slip on the snakeboard foot-pads. With this assumption, the foot-pads follow the hip joint trajectories.*

B. Snakeboard X-Y controller

To achieve a desired displacement in the XY plane, we consider a modified version of the *drive* gait. In particular, we consider the following desired trajectories for the hip joints and pelvis yaw,

$$q^d_{hip,f}(t) = c + a\sin(wt),\ q^d_{hip,b}(t) = -a\sin(wt), \tag{17}$$

$$\theta^d_c(t) = a\sin(wt), \tag{18}$$

with $c = -K_x(x_s - x^d_s) - D_x(\dot{x}_s - \dot{x}^d_s)$, where x^d_s represents the desired x location. This controller prevents the board from drifting too far from the desired x-direction.

C. Velocity Controller

Velocity control is accomplished by regulating the amplitude of the sinusoids in (17)-(18) given by the proportional feedback law,

$$a = -K_v(v_s - v^d_s), \tag{19}$$

where $v_s = \sqrt{\dot{x}^2_s + \dot{y}^2_s}$ represents the magnitude of the velocity of the snakeboard.

D. Turning Controller

The turning controller maintains a desired heading angle θ^d_s of the snakeboard. We consider the following gait for the desired hip angles q^d_{hip},

$$q^d_{hip,f} = c + a\sin(wt),\ q^d_{hip,b} = -c - a\sin(wt), \tag{20}$$

where $c = -K_\theta(\theta_s - \theta^d_s) - D_\theta(\dot{\theta}_s - \dot{\theta}^d_s)$.

To account for sharp turns, Cassie would need to lean in the direction of the turn to ensure stability and balance on the snakeboard. To further analyze this, we consider an inverted pendulum model in Fig. 2 that represents Cassie's center-of-mass. Here, F_s and F_n denote the tangential and normal forces acting at the contact points, and $F_c = \frac{mv^2}{R}$ denotes the centripetal force at the center-of-mass.

Using a comparable model to the snakeboard studied by [21], the radius of curvature of the trajectory R can be calculated as,

$$R = \frac{2l}{(\tan\phi_f - \tan\phi_b)\cos\omega}, \tag{21}$$

$$\omega = \arctan\frac{\tan\phi_b + \tan\phi_f}{2}, \tag{22}$$

where ω represents the slip angle at the center-of-mass of the board and l represent the length of the center-of-mass of the snakeboard to the foot-pad. Summing up the moment about point O in Fig. 2 the desired lean angle θ^d_l for Cassie is given by

$$\theta_l = \arctan\frac{v^2}{gR}. \tag{23}$$

To achieve the desired lean angle θ_l, we consider the following desired center-of-mass position with respect to the snakeboard r^d_c for Cassie in (14) as,

$$r^d_c = \Delta z \begin{bmatrix} \sin\theta_l\cos\theta_s \\ \sin\theta_l\sin\theta_s \\ \cos\theta_l \end{bmatrix}, \tag{24}$$

where Δz is the difference between a nominal desired height of Cassie from the ground and the height of the snakeboard's foot-pads from the ground.

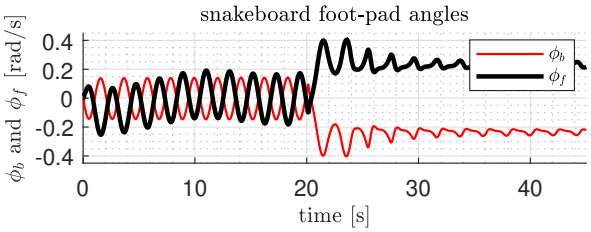

(a)

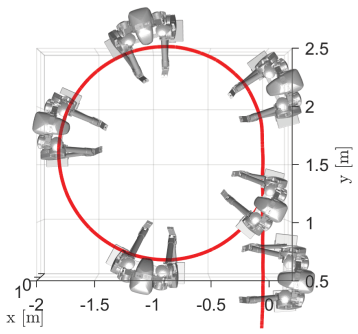

(b)

Fig. 6: Results for tracking a circular path in Section V-B. (a) Foot-pad angles of the snakeboard. (b) Center-of-mass position of the snakeboard.

V. Simulation Results

Having presented the dynamics of the Cassie-snakeboard system and a feedback controller for regulating the inertial position and orientation, we now present results from numerical simulation for various scenarios.

A. Velocity Tracking

In this section, we consider regulating the velocity of the Cassie-snakeboard system while following a straight line. This is achieved by the control strategies presented in Section IV-B and Section IV-C. Fig. 5 illustrates the results of velocity tracking of the forward velocity of the Cassie-snakeboard system.

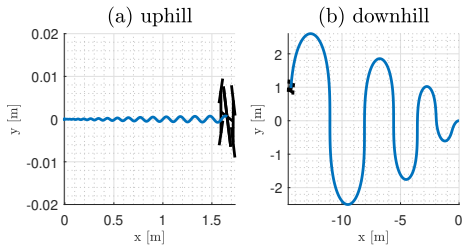

Fig. 7: Numerical simulation results for the simplified snakeboard model moving (a) uphill and (b) downhill.

B. Turning Controller - Circular Path

The turning controller utilizes both, the velocity and the turning controllers. Fig. 6 illustrates the results from a numerical simulation of the turning controller. In this particular case, we consider the desired heading angle to be $\theta_s^d(t) = 0.2t + \theta_0,\ t > 15s$ where $\theta_0 = \pi/2$. For $t \leq 15$ we use the velocity controller to follow a straight path and build up speed.

C. Turning Controller - Sinusoidal Path

We consider a sinusoidal trajectory that requires Cassie to make sharp turns without slipping and illustrate the importance of leaning during sharp turns. In this example, we consider an initial velocity of 0.8m/s for the Cassie-snakeboard system and a desired heading angle $\theta_s^d = 0.8\sin t + \theta_0$ where $\theta_0 = \pi/2$.

For the case without leaning into a turn, Cassie slips within a few seconds as can be seen in Fig. 8 (top-right), which shows that the ratio between the sum of the horizontal forces over the normal force exceeded the coefficient of static friction. However, for the case where the robot was able to lean, Cassie is able to maneuver itself into sharp turns while still ensuring the friction constraints are satisfied, as shown in Fig. 8 (top-left).

D. Obstacle Avoidance

For avoiding obstacles in the task-space, we begin by defining a path that geometrically avoids the obstacles. Then, by utilizing the XY controller, we can follow the trajectory to avoid obstacles. Fig. 9 shows a simulation of the Cassie-snakeboard system avoiding two different obstacles in the shape of a sphere with a radius of 0.2m. To achieve this, we consider the piece-wise function for the desired x position as a function of y,

$$x_s^d = 0.3\sin(y_s - y_0), \tag{25}$$

where the particular values of y_0 are obtained by considering the position of the obstacles. In this particular case, Cassie's initial velocity is equal to 0.2m/s.

VI. Future Work

As part of future work, we plan to implement the proposed controller on hardware. We also seek to explore robots with an upper torso and arms, like Digit [2], to broaden the range

[2] https://www.agilityrobotics.com/meet-digit

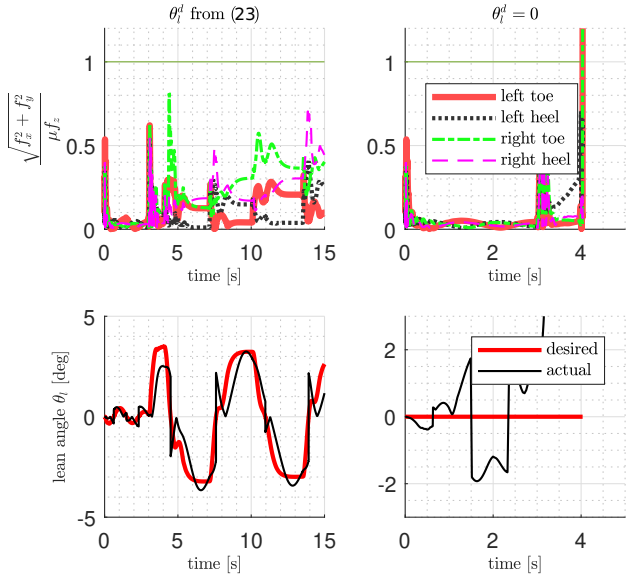

Fig. 8: Simulation results for sinusoidal trajectory in Sec. V-C with (left column) and without (right column) leaning into sharp turns.

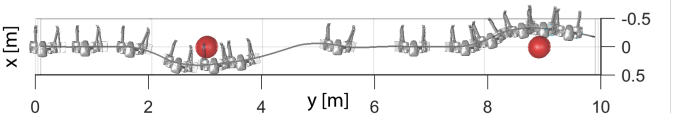

Fig. 9: Center-of-mass position of the snakeboard while avoiding obstacles (in red).

of achievable motions. Another potential future direction is to analyze the problem of negotiating inclines. Towards this goal, we analyzed the dynamics of the simplified model of the snakeboard on surfaces of a constant incline angles. With the assumption that the ground makes a constant angle α with the $x-$axis, the Lagrangian of the snakeboard can be written as

$$L = \frac{1}{2}(m_s + m_r)\left(\dot{x_s}^2 + \dot{y_s}^2\right) + \frac{1}{2}J\dot{\theta}_s^2 + \frac{1}{2}J_r\left(\dot{\psi} + \dot{\theta}_s\right)^2 + \frac{1}{2}J_w\left(\left(\dot{\phi}_b + \dot{\theta}_s\right)^2 + \left(\dot{\phi}_f + \dot{\theta}_s\right)^2\right) - (m_s + m_r)gx_s\sin\alpha, \tag{26}$$

where g denotes the acceleration due to gravity. Fig. 7 illustrates the drive gait from Section III for going up and downhill with the simplified snakeboard dynamics. As part of future work, we plan to investigate navigation on severe inclines and dynamic *hybrid* motions like flips and jumps with the snakeboard.

VII. Conclusion

In this paper, we presented a gait generation technique and feedback controller for a bipedal robot to autonomously ride an unpowered wheeled platform called Snakeboard, which is a steerable variant of a Skateboard. Our proposed controller is able to achieve sharp turns, navigate around an obstacle course and follow desired trajectories in the task space.

REFERENCES

[1] S. Chen, J. Rogers, B. Zhang, and K. Sreenath, "Feedback control for autonomous riding of hovershoes by a cassie bipedal robot," in *2019 IEEE-RAS 19th International Conference on Humanoid Robots (Humanoids)*, 2019, pp. 1–8.

[2] Y. Gong, R. Hartley, X. Da, A. Hereid, O. Harib, J.-K. Huang, and J. Grizzle, "Feedback control of a cassie bipedal robot: Walking, standing, and riding a segway," in *American Control Conference*, 2019, pp. 4559–4566.

[3] M. Bjelonic, C. D. Bellicoso, Y. de Viragh, D. Sako, F. D. Tresoldi, F. Jenelten, and M. Hutter, "Keep rollin'—whole-body motion control and planning for wheeled quadrupedal robots," vol. 4, no. 2, 2019, pp. 2116–2123.

[4] V. Klemm, A. Morra, C. Salzmann, F. Tschopp, K. Bodie, L. Gulich, N. Küng, D. Mannhart, C. Pfister, M. Vierneisel, F. Weber, R. Deuber, and R. Siegwart, "Ascento: A two-wheeled jumping robot," in *2019 International Conference on Robotics and Automation*, 2019, pp. 7515–7521.

[5] S. Chen, K. Huang, W. Chen, S. Shen, C. Li, and P. Lin, "Quattroped: A leg–wheel transformable robot," *IEEE/ASME Transactions on Mechatronics*, vol. 19, no. 2, pp. 730–742, 2014.

[6] Y. Zheng and K. Yamane, "Ball walker: A case study of humanoid robot locomotion in non-stationary environments," in *2011 IEEE International Conference on Robotics and Automation*, 2011, pp. 2021–2028.

[7] C. Yang, B. Zhang, J. Zeng, A. Agrawal, and K. Sreenath, "Dynamic legged manipulation of a ball through multi-contact optimization," *arXiv preprint arXiv:2008.00191*, 2020.

[8] N. Takasugi, K. Kojima, S. Nozawa, F. Sugai, K. Yohei, K. Okada, and M. Inaba, "Extended three-dimensional walking and skating motion generation for multiple noncoplanar contacts with anisotropic friction: Application to walk and skateboard and roller skate," *IEEE Robotics and Automation Letters*, vol. 4, no. 1, pp. 9–16, 2018.

[9] J. Ostrowski, A. Lewis, R. Murray, and J. Burdick, "Nonholonomic mechanics and locomotion: the snakeboard example," in *IEEE International Conference on Robotics and Automation*, 1994, pp. 2391–2397.

[10] J. P. Ostrowski, J. P. Desai, and V. Kumar, "Optimal gait selection for nonholonomic locomotion systems," *The International journal of robotics research*, vol. 19, no. 3, pp. 225–237, 2000.

[11] F. Bullo and K. M. Lynch, "Kinematic controllability for decoupled trajectory planning in underactuated mechanical systems," *IEEE Transactions on Robotics and Automation*, vol. 17, no. 4, pp. 402–412, 2001.

[12] F. Bullo and A. D. Lewis, "Kinematic controllability and motion planning for the snakeboard," *IEEE Transactions on Robotics and Automation*, vol. 19, no. 3, pp. 494–498, 2003.

[13] E. A. Shammas, H. Choset, and A. A. Rizzi, "Towards a unified approach to motion planning for dynamic underactuated mechanical systems with non-holonomic constraints," *The International Journal of Robotics Research*, vol. 26, no. 10, pp. 1075–1124, 2007.

[14] E. Shammas and M. De Oliveira, "Motion planning for the snakeboard," *The International Journal of Robotics Research*, vol. 31, no. 7, pp. 872–885, 2012.

[15] T. Dear, R. L. Hatton, M. Travers, and H. Choset, "Snakeboard motion planning with local trajectory information," in *Dynamic Systems and Control Conference*, vol. 56130. American Society of Mechanical Engineers, 2013, p. V002T33A002.

[16] T. Dear, S. D. Kelly, M. Travers, and H. Choset, "Snakeboard motion planning with viscous friction and skidding," in *2015 IEEE International Conference on Robotics and Automation (ICRA)*. IEEE, 2015, pp. 670–675.

[17] A. Agrawal, H. M. Zaini, T. Dear, and H. Choset, "Experimental gait analysis of waveboard locomotion," in *Dynamic Systems and Control Conference*, vol. 50701. American Society of Mechanical Engineers, 2016, p. V002T22A011.

[18] C. Ott, M. A. Roa, and G. Hirzinger, "Posture and balance control for biped robots based on contact force optimization," in *IEEE-RAS International Conference on Humanoid Robots*, 2011, pp. 26–33.

[19] Y. Gong, R. Hartley, X. Da, A. Hereid, O. Harib, J.-K. Huang, and J. Grizzle, "Feedback control of a cassie bipedal robot: Walking, standing, and riding a segway," in *2019 American Control Conference (ACC)*. IEEE, 2019, pp. 4559–4566.

[20] H. Dai and R. Tedrake, "Planning robust walking motion on uneven terrain via convex optimization," in *2016 IEEE-RAS 16th International Conference on Humanoid Robots (Humanoids)*. IEEE, 2016, pp. 579–586.

[21] R. Rajamani, "Lateral vehicle dynamics," in *Vehicle Dynamics and control*. Springer, 2012, pp. 15–46.